

# Strain-induced band gap engineering in layered $\text{TiS}_3$

Robert Biele<sup>1</sup> (✉), Eduardo Flores<sup>2</sup>, Jose Ramón Ares<sup>2</sup>, Carlos Sanchez<sup>2,3</sup>, Isabel J. Ferrer<sup>2,3</sup>, Gabino Rubio-Bollinger<sup>3,4</sup>, Andres Castellanos-Gomez<sup>5</sup> (✉), and Roberto D'Agosta<sup>1,6</sup> (✉)

<sup>1</sup> Nano-Bio Spectroscopy Group and European Theoretical Spectroscopy Facility (ETSF), Universidad del País Vasco, 20018 San Sebastián, Spain

<sup>2</sup> Materials of Interest in Renewable Energies Group (MIRE Group), Dpto. de Física de Materiales, Universidad Autónoma de Madrid, 28049 Madrid, Spain

<sup>3</sup> Instituto de Ciencia de Materiales "Nicolás Cabrera", Campus de Cantoblanco, 28049 Madrid, Spain

<sup>4</sup> Dpto. de Física de la Materia Condensada, Condensed Matter Physics Center (IFIMAC), Universidad Autónoma de Madrid, Campus de Cantoblanco, 28049 Madrid, Spain

<sup>5</sup> Instituto de Ciencia de los Materiales de Madrid (ICMM-CSIC), Cantoblanco, 28049 Madrid, Spain

<sup>6</sup> IKERBASQUE, Basque Foundation for Science, 48013 Bilbao, Spain

Received: 23 January 2017

Revised: 8 April 2017

Accepted: 11 April 2017

© Tsinghua University Press  
and Springer-Verlag GmbH  
Germany 2017

## KEYWORDS

band gap engineering,  
titanium trisulfide,  
2-D materials,  
strain

## ABSTRACT

By combining *ab initio* calculations and experiments, we demonstrate how the band gap of the transition metal trichalcogenide  $\text{TiS}_3$  can be modified by inducing tensile or compressive strain. In addition, using our calculations, we predicted that the material would exhibit a transition from a direct to an indirect band gap upon application of a compressive strain in the direction of easy electrical transport. The ability to control the band gap and its nature could have a significant impact on the use of  $\text{TiS}_3$  for optical applications. We go on to verify our prediction via optical absorption experiments that demonstrate a band gap increase of up to 9% (from 0.99 to 1.08 eV) upon application of tensile stress along the easy transport direction.

## 1 Introduction

The discovery of graphene [1] paved the way for the investigation into a vast class of materials, whose salient characteristic is to exist in a single, (or a few) layer(s). For example, similar to graphene, the existence of silicene and germanene were predicted and later

confirmed [2–4]. At the same time, the mechanical exfoliation technique that allowed the breakthrough in producing graphene from graphite, also allowed the production of single (or a few) layer(s) materials derived from other sources. One family of these materials is the transition metal dichalcogenides (TMDs), e.g.,  $\text{MoS}_2$ ,  $\text{MoSe}_2$ ,  $\text{WS}_2$ , and  $\text{WSe}_2$ . TMDs have

Address correspondence to Robert Biele, r.biele02@gmail.com; Andres Castellanos-Gomez, andres.castellanos@imdea.org; Roberto D'Agosta, roberto.dagosta@ehu.es

shown semiconductor properties, like a direct band gap and electrical tunability, superior (to a certain extent) to those of graphene, and could form the basis for novel transistors and photodetectors. Ideally, these materials should have a band gap comparable to that of silicon to simplify their integration into current devices for technological applications. TMD band gaps are likely too large for use in photovoltaic, photocatalytic, or photodetector devices and, in addition, potential thermoelectric applications usually require narrow band semiconductors. However, TMDs possess a direct band gap only when reduced to a single layer material, due to interlayer interactions. On the other hand, transition metal trichalcogenides (TMTs) can be reduced to single or a few layer materials while maintaining a direct band gap of about 1 eV [5]. In particular titanium tri-sulfide,  $\text{TiS}_3$ , presents a direct band gap of about 1 eV [6] and an extremely fast optical response: an ideal property for the next generation of photodetectors [7–9]. Moreover, it has been predicted that  $\text{TiS}_3$  could be a promising electrode material for Li and Na ion batteries [10], photoelectrodes for  $\text{H}_2$  photogeneration [11], and nano-electronics and optics [12]. It also presents strong anisotropic behavior and non-linearity, in both the electronic and optical properties [8, 9, 13, 14]. The exfoliation of a single-layer of  $\text{TiS}_3$  is a relatively recent achievement [7]. It has also been shown that by controlling the growth conditions one can obtain different materials, from nano-ribbons to flakes, as well as tailoring several of the electrical properties of  $\text{TiS}_3$ . In particular, the presence of S vacancies has an important effect on the electronic transport properties of nano-ribbons consisting of a few layers [8, 15]. In this work, we show that one can control the electronic band gap by inducing compressive or tensile uniaxial strain in the material. Recently, a lot of attention has been focused on band gap modulations induced by tensile strain. Those studies investigated the theoretical band gap changes when the material was subjected to tensile strain only [16–20]. However, experimental verification of this, and a theoretical investigation into compressive strain effects, are still missing. Here, we consider the cases of mono- and bi-layer  $\text{TiS}_3$ , and show that one can induce a direct-to-indirect band gap transition by inducing compressive strain into the electronic easy

transport direction. Similar transitions have been reported for other monolayer materials; the possibility of controlling the band gap via induced strain is also explored [21–25]. We test our prediction by stretching a thin  $\text{TiS}_3$  sample and measuring its band gap via optical absorption spectroscopy.

## 2 Results and discussion

We calculated the electronic band structure of mono- and bi-layer  $\text{TiS}_3$ , with their atomic configurations detailed in Fig. 1. (See the section 4.1 for details on these calculations, and more information about the atomic structure.) We found that they are direct gap semiconductors with a density functional theory (DFT) gap of around 0.31 eV (monolayer) and 0.27 eV (bilayer). A more refined calculation based on non-self-consistent  $G_0W_0$  ( $G_0$  is Green's function,  $W_0$  is the interaction) approximation increases the gap to the experimental levels of about 1.3 eV for the monolayer.

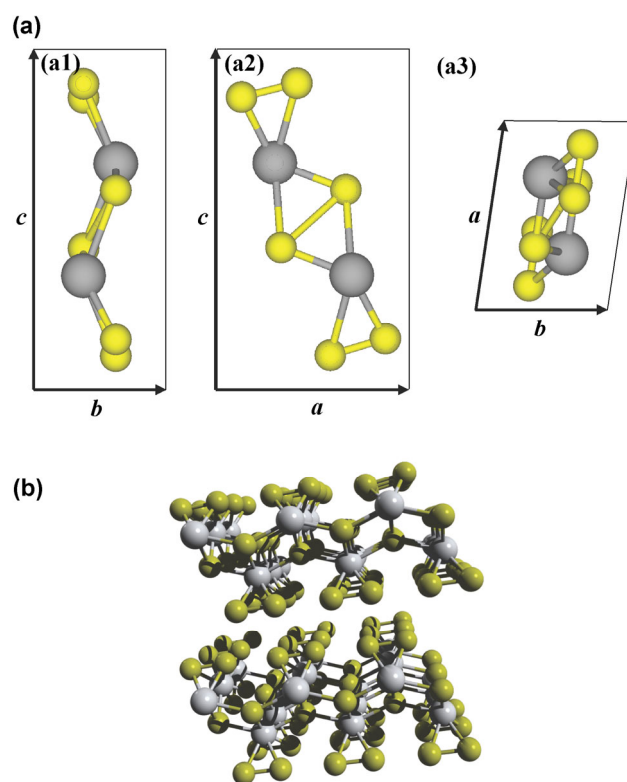


**Figure 1** Sketch of the atomic structures: (a) the unit cell of  $\text{TiS}_3$  and (b) the bi-layer under investigation (Ti in gray, S in yellow/gold). On top, we show the projection of the unit cell atomic positions along the  $a$  (a1),  $b$  (a2), and  $c$  (a3) directions, respectively.

Note that, due to quantum confinement effects, the band gap increases when moving from the bulk material (0.99–1.1 eV) [8, 26] to the monolayer (1.3 eV). In order to study strain-induced band gap modulation, we applied a stress by deforming the length of the unit-cell vector in the  $a$  or  $b$  direction and relaxed the atomic positions. We neglected the effect of the Poisson's deformation induced in the other two axes of the unit cell. Preliminary results have shown this effect to be negligible with Poisson's ratios of the order of 0.04–0.08. (These results will be presented elsewhere.)

In Fig. 2 one can see the normalized band gap change  $\Delta E/E_0$  for  $\text{TiS}_3$ . Here,  $E_0$  refers to the band gap of the material when no strain is applied, while  $\Delta E$  is the change in the electronic gap with respect to  $E_0$  when strain is applied. For both systems, a tensile strain in  $b$  direction increases the band gap monotonically. Most interestingly, a compression in the same direction leads to a reduction in the direct gap by up to  $-3\%$ , applying  $-4\%$  or more strain transforms the gap to an indirect one by keeping the gap constant at around one third of its original value. This direct-indirect transition might have important consequences in tailoring the optical response of possible  $\text{TiS}_3$  based phototransistors. In addition, applying a tensile strain up to  $5\%$  along  $a$  reduces the direct gap, whilst applying

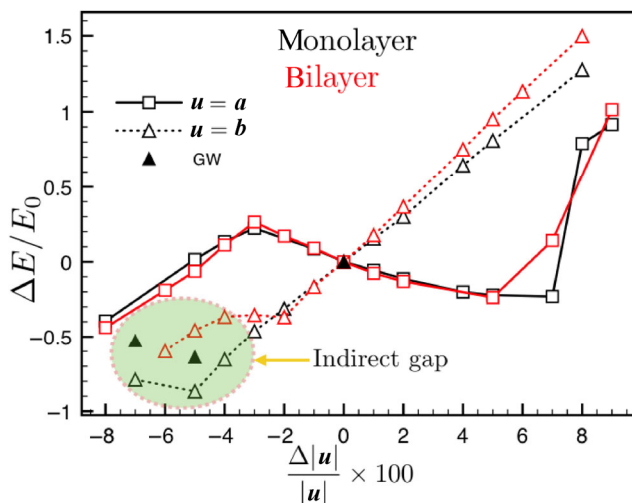


**Figure 2** Modulation of the direct band gap of mono- (black) and bi-layer (red)  $\text{TiS}_3$  by applying tensile or compressive strain, along the unit cell vector  $a$  or  $b$ . All gaps are direct except for the green shaded area: A direct to indirect gap transition is predicted when negative strain of around  $-4\%$  is applied in the  $b$  direction. Here,  $E_0$  is the band gap of  $\text{TiS}_3$  when strain has not been applied.

any greater strain increases the gap. Notably, a compressive strain in the same direction first increases the gap (until  $3\%$ ), and then decreases it monotonically. These findings are unique as, for TMDs, a tensile strain always reduces the band gap [27]. In order to prove the validity of our DFT results, we performed calculations based on the  $G_0W_0$  approximation and found that  $G_0W_0$  opens up the band gap of the mono- and bi-layer material uniformly, for both strained and unstrained cases. The interesting direct-indirect transition found in this work was also reproduced by the  $G_0W_0$  approximation.

To better understand this transition, the  $G_0W_0$  band structures for the unstrained and  $5\%$  strained along  $b$  monolayer are shown in Fig. 3. We clearly see that the conduction band is almost untouched by the compression, while the valence bands develop a local maximum between  $\Gamma$  and  $X'$ , reducing the gap and

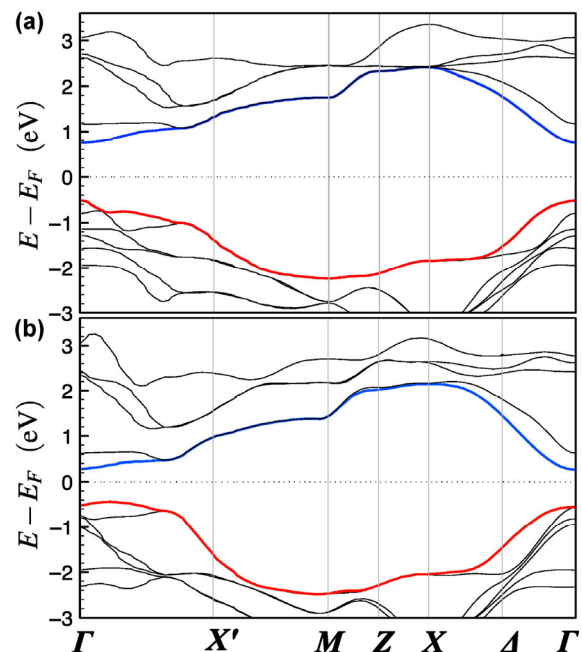


**Figure 3**  $\text{TiS}_3$  electronic bands for the monolayer, unstrained unit cell structure (a), and the  $5\%$  compressed unit cell in the  $b$  direction (b). Represented in blue and red respectively are the conduction and valence bands. The upper plot (a), corresponding to the unstrained unit cell, shows a direct gap at the  $\Gamma$ -point. The compressed structure, lower plot (b), shows a decreased indirect gap between  $\Gamma$  and  $X'$ . All of the energies have been rescaled to the Fermi energy  $E_F$ . The path for the calculations was delimited by the high-symmetry points  $\Gamma = (0, 0)$ ,  $X' = (1/2, 0)$ ,  $M = (1/2, -1/2)$ ,  $X = (0, -1/2)$ , and the intermediate points  $Z = (1/4, -1/2)$  and  $\Delta = (0, -1/4)$ .

changing its nature. Interestingly, the reduction of the band gap in the transition from the direct to indirect gap is more marked here compared to previous reports on  $\text{TiS}_3$  nanoribbons under tensile strain. In those cases, the band gap modification was only of a few meV [17], and in certain instances, below the accuracy of the pseudopotentials used in DFT calculations.

Finally, to understand the different behaviors of the material under uniaxial strain in the two directions, we report in Fig. 4 the highest occupied (HO), top, and lowest unoccupied (LU), bottom, Kohn–Sham orbital densities. As illustrated, the HO density is mostly aligned along the Ti–S bond in the  $a$  direction, while the LU density is essentially concentrated on the Ti atoms. If we compress the material in the  $b$  direction, the overall energy of the HO increases due to the Coulomb repulsion. For the same compression, the LU energy remains essentially unchanged. Therefore, we expect that a compression in the  $b$  direction decreases the gap at the  $\Gamma$  point.

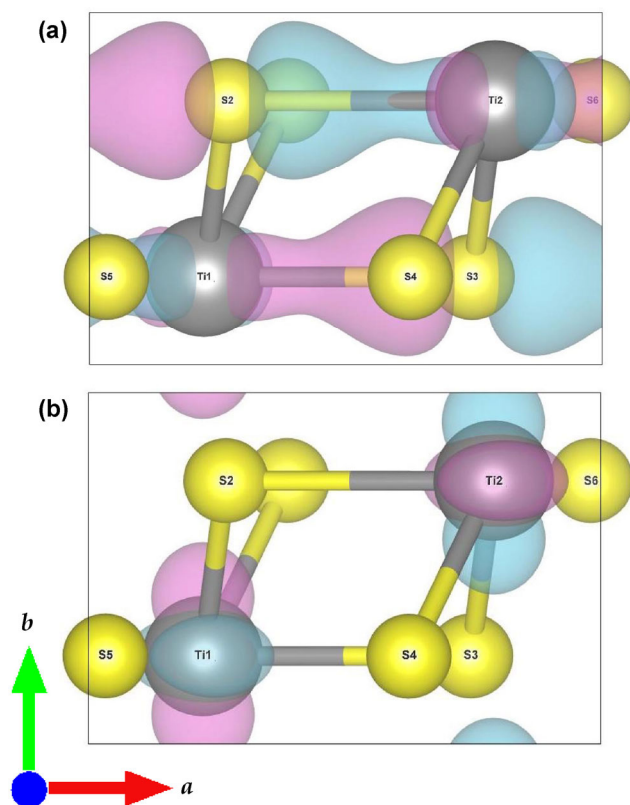


**Figure 4** (a) Projection of the HO and (b) LU in a single unit cell for a  $\text{TiS}_3$  monolayer along the vertical axis. Ti atoms are in grey and S atoms in yellow. Electronic densities are in purple and light blue.

In order to experimentally verify the predicted effect of strain on the electronic band structure of  $\text{TiS}_3$ , we investigated the optical absorption spectra of a thin  $\text{TiS}_3$  ribbon subjected to uniaxial strain. (See section 4.2 for details about the growth of this material.) The strain was applied by exploiting the buckling-induced delamination process that takes place when a thin elastic film, deposited onto an elastomeric substrate, is subjected to a uniaxial compressive strain [28, 29]. The juxtaposition between the bending rigidity of the thin-film and the thin-film/elastomeric substrate adhesion forms wrinkles that delaminates the material from the elastomeric substrate, where the thin-film is uniaxially stretched. (We direct the reader to the following reference for a more in-depth discourse on the buckling-induced delamination process [30].) Figure 5(a) depicts the process followed in fabricating a uniaxially strained  $\text{TiS}_3$  sample. A gel-film substrate (a commercially available elastomeric substrate) is uniaxially stretched by 30%, then  $\text{TiS}_3$  is deposited onto the stretched surface and the strain is suddenly released, leading to the buckling-induced delamination of  $\text{TiS}_3$  (see Fig. 5(b)), creating both flat regions (released stress) and delaminated wrinkles (accumulated tensile stress). According to Vella et al. [31], the tensile stress can be estimated by

$$\varepsilon \sim \pi^2 h \delta / (1 - \sigma^2) \lambda^2 \quad (1)$$

where  $\sigma$  is the Poisson's ratio, which in our case is small,  $h$  is the thickness of the flake, and  $\delta$  and  $\lambda$  are the height and width of the wrinkle, respectively. The stress is uniaxial and is applied along the direction perpendicular to the wrinkles. In this work, the wrinkles are parallel to the  $a$  direction of the  $\text{TiS}_3$  lattice, indicating that the tensile stress is along the  $b$  direction. For thin  $\text{TiS}_3$  ribbons (10 to 30 nm thick, like the one investigated here) the wrinkles were 100–300 nm in height, with an estimated maximum tensile strain on the topmost part in the order of 0.3%–0.7% [28, 31]. The change in the band structure induced by the applied uniaxial strain along  $b$  was probed by a recently developed hyper-spectral imaging technique based on absorption spectroscopy [32]. Figure 5(c) shows the absorption spectra,  $\alpha^2$ , acquired from 9 flat regions and the tops of 4 wrinkles. The intercept of the relationship  $\alpha^2$  vs.  $E$ , with the

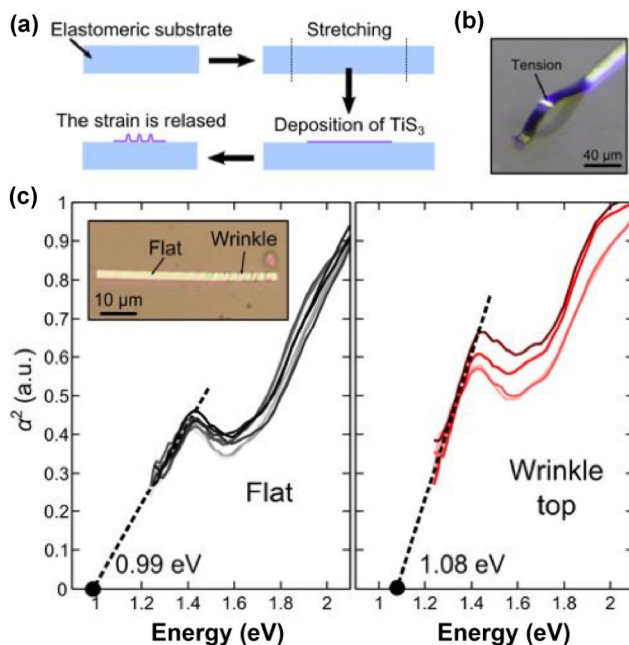


**Figure 5** (a) Schematic diagram of the steps employed to fabricate uniaxially strained  $\text{TiS}_3$  by exploiting the buckling-induced delamination process. (b) High-angle optical microscopy image of a delaminated wrinkle occurring on a thin  $\text{TiS}_3$  ribbon. (c) Optical absorption spectra acquired on nine different flat regions (left) and on the topmost part of four wrinkles on a thin  $\text{TiS}_3$  ribbon (shown in the inset). The intercept with the horizontal axis indicates the estimated band gap value for the different regions.

horizontal axis, gives an estimate of the band gap (valid only for direct gap semiconductors, for indirect gap semiconductors it should be  $\alpha^{1/2}$  vs.  $E$ ). The band gap value obtained for the flat regions, 0.99 eV, was in good agreement with the value determined by conventional absorption spectroscopy, and by photocatalysis measurements on the bulk material [6, 9]. For the topmost part of the wrinkles, the slope of the absorption band edge increases considerably, yielding an estimated band gap value of 1.08 eV, 90 meV higher than the unstrained  $\text{TiS}_3$ . This experimental observation proves that 0.3%–0.7% uniaxial tensile strain along  $\mathbf{b}$  changes the local band structure by opening the band gap, without changing its nature, which remains direct (as evidenced by the marked linear behavior of the absorption band edge in the representation  $\alpha^2$  vs.  $E$ ). The experimental value also confirms the high sensitivity to compression or expansion of these samples, as predicted by our calculations. From Fig. 2, one can infer for small amplitude strain, the linear relation  $\Delta E/E_0 \approx g\Delta|u|/|u|$ , with the “gauge factor”

$g = 20$  for strain in the  $\mathbf{b}$  direction. This was in relatively good agreement with the experimental value, where we estimated  $g$  to be in the range of 13 to 30. In comparison to other materials, we observe that  $\text{TiS}_3$  has quite a large value for  $g$ , for example: a monolayer of  $\text{MoS}_2$  has  $g = 10$  [23], arsenene has  $g = 8$  [25], while bulk black phosphorus has  $g = 20$  [33]. Note that the large uncertainty in the experimentally determined strain tunability stems from difficulty in estimating the actual strain applied to the sample. Additionally, we note that for low strain values, such as those in our experiment, the exciton binding energy is considerably small, and hence, it can be neglected [9].

### 3 Conclusions

In conclusion, we have carried out a systematic investigation of the band gap modification of mono- and bi-layer  $\text{TiS}_3$  when the system is subjected to strain.  $G_0W_0$  calculations predicted a band gap comparable with the experimental value ( $\sim 1.3$  eV). We found that the band gap could be controlled by inducing strain in certain directions along the primitive axes of the unit cell. Most interestingly, we found that the band gap of the monolayer and bilayer material changed from direct to indirect, when compressive strain was induced along the preferred transport axis ( $\mathbf{b}$  in Fig. 1). We tested these predictions by inducing strain in a  $\text{TiS}_3$  sample; the band gap was shown to increase when the system was under tensile strain, in agreement with the predictions detailed in Fig. 2. This behavior was most notable for two reasons: the band gap for two-dimensional dichalcogenide materials always closes under tensile strain and, this alternative behavior may lead to a number of novel applications of  $\text{TiS}_3$ .

### 4 Methods

#### 4.1 Theory

To calculate the electronic band structure, we performed state-of-the-art DFT calculations in combination with many-body techniques. The DFT calculations were performed with a pseudopotential plane-wave method, as implemented in the Quantum-ESPRESSO suite [34]. For both Ti and S, the electron exchange-correlation

potential is evaluated within the generalized gradient approximation throughout the Perdew–Burke–Ernzerhof functional. For S, the Martins–Troulliers’ pseudopotential was used, while for Ti, the Goedecker–Hartwigsen–Hutter–Teter pseudopotential, including semi-core states for the valence electrons, was used [35, 36]. These pseudopotentials are norm-conserving and scalar-relativistic. By starting from the experimental parameters for the unit cell [8] and the spectroscopic atomic configuration (monoclinic,  $P2_1/m$ ) [37], we optimized the atomic positions with a residual force after relaxation of 0.001 a.u. using the Broyden–Fletcher–Goldfarb–Shanno scheme. This relaxation procedure for the bulk unit cell gives  $|a| = 4.989 \text{ \AA}$ ,  $|b| = 3.435 \text{ \AA}$ ,  $|c| = 8.675 \text{ \AA}$ , and an angle between  $a$  and  $c$ ,  $\beta = 97.132^\circ$ , in good agreement with experimental values [8]. The kinetic energy cutoff for the plane wave basis set was fixed at 220 Ry, while the cutoff for the charge density was 880 Ry. Sampling of the Brillouin zone for the material is  $14 \times 14 \times 14$ , according to the Monkhorst–Pack scheme. These parameters were chosen to ensure convergence of the band gap within an accuracy of around 0.01 eV. We have not included van der Waals corrections in these calculations because, from our previous experience, we observed that they have an essentially negligible effect on the electronic bands. To support this statement, we have calculated the band structure for the bilayer in the presence of van der Waals corrections. As detailed in Fig. 6, especially at the  $\Gamma$  point, the band structure is the same, regardless of van der Waals corrections.

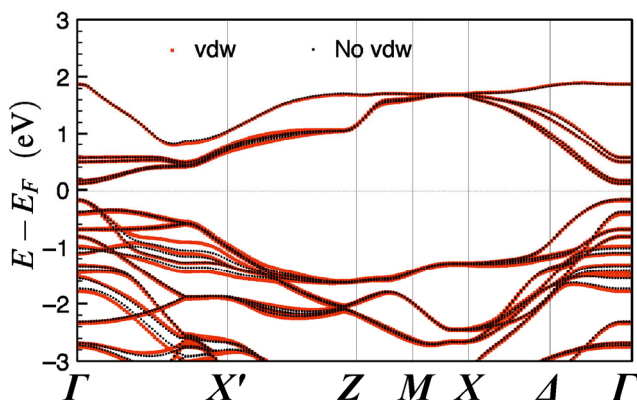


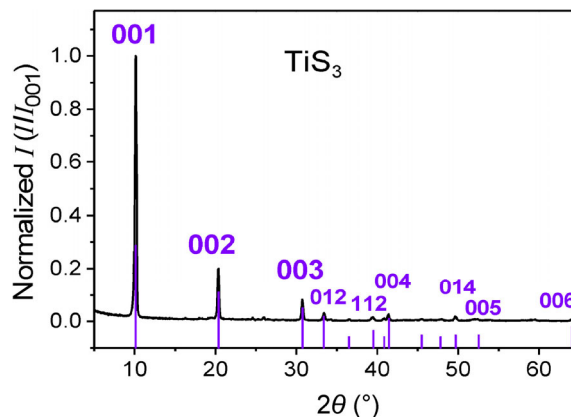
**Figure 6** The electronic band structure for the  $\text{TiS}_3$  bilayer with (red), and without (black), van der Waals corrections.

Indeed, their main effect is an expansion in the  $c$  direction, however, that is irrelevant when considering the mono- and bi-layer band structure. As DFT calculations tend to underestimate the band gap, we performed additional quasi-particle corrections on top of these, within the more accurate  $G_0W_0$  approximation for the monolayer case. With the results obtained within the  $G_0W_0$  approximation, we were able to judge whether the DFT band gaps could be qualitatively trusted or not. We found that the  $G_0W_0$  approximation opens up the band gaps uniformly, but does not change the nature of the gaps. Within the  $G_0W_0$  approximation, we converged the band gap with an accuracy of around 0.05 eV.

## 4.2 Synthesis and characterization

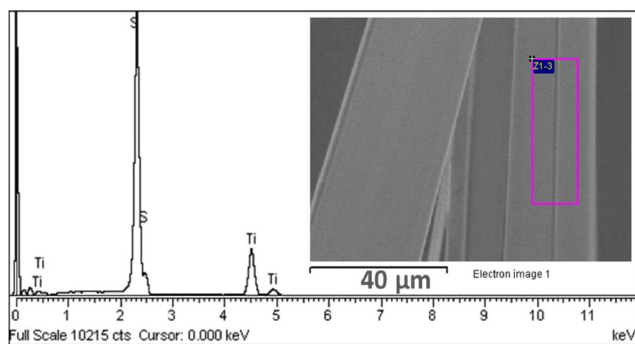
$\text{TiS}_3$  was synthesized by a solid-gas reaction between Ti powder (Goodfellow, 99.5% purity) and sulfur gas obtained by heating sulfur powder (Merck, 99.75% purity) in a vacuum sealed ampoule at  $550^\circ\text{C}$  over 15 days. The S:Ti molar ratio in the ampoule was 3:1. The compound obtained was characterized by X-ray Diffraction (XRD) using a Siemens D5000 Automated X-ray diffractometer with Cu K  $\alpha$ -radiation ( $\lambda = 1.5406 \text{ \AA}$ ). The product displayed a unique crystalline phase identified as monoclinic ( $P211/m1$ )  $\text{TiS}_3$  according to the reference pattern (JCPDS ICDD 36-1337).

Figure 7 shows the XRD pattern for the obtained powder product. Miller’s indices for  $\text{TiS}_3$  have also been included in the plot. Morphology and composition were analyzed by Scanning Electron Microscopy (SEM, mod. Hitachi S-3000N) coupled to an Energy Dispersive



**Figure 7** XRD pattern of  $\text{TiS}_3$  powder and Miller’s indices according to JCPDS ICDD 36-1337.

Analyzer of X-ray (EDX. mod. INCA X-sight). Incident electron beam energy was 10 KeV. The average S:Ti ratio obtained from the EDX results was  $3.07 \pm 0.05$  (see Fig. 8). Figure 8 shows one of the EDX spectra and the corresponding image of the  $\text{TiS}_3$  belts, including the zone where the analysis was performed.



**Figure 8** EDX spectrum of the  $\text{TiS}_3$  ribbon obtained from the zone indicated in the SEM image (inset).

## Acknowledgements

R. B. and R. D'A. acknowledge financial support by the projects DYN-XC-TRANS (No. FIS2013-43130-P), SELECT-DFT (No. FIS2016-79464-P), the Grupo Consolidado UPV/EHU del Gobierno Vasco (No. IT578-13), and NANOTerm (No. CSD2010-00044) of the Ministerio de Economía y Competitividad (MINECO). R. B. acknowledges the financial support of Ministerio de Educación, Cultura y Deporte (No. FPU12/01576). R. D'A. is grateful to the Physics Department of King's College London for its hospitality during the completion of this work supported by the Grant No. MV-2015-1-17 of the Diputación Foral de Guipuzkoa. A.C.-G. acknowledges financial support from the European Commission under the Graphene Flagship, contract CNECTICT-604391 and from the MINECO (Ramón y Cajal 2014 program RYC-2014-01406 and MAT2014-58399-JIN) and from the Comunidad de Madrid (MAD2D-CM Program (S2013/MIT-3007)). G.R.-B. acknowledges financial support from the Grant No. MAT2014-57915-R from the MINECO. The MIRE group acknowledges financial support from MINECO (No. MAT2015-65203R) and E. F. thanks the Mexican National Council for Science and Technology (CONACyT) for providing a PhD. Grant.

## References

- [1] Novoselov, K. S.; Geim, A. K.; Morozov, S. V.; Jiang, D.; Zhang, Y.; Dubonos, S. V.; Grigorieva, I. V.; Firsov, A. A. Electric field effect in atomically thin carbon films. *Science* **2004**, *306*, 666–669.
- [2] Cahangirov, S.; Topsakal, M.; Aktürk, E.; Şahin, H.; Ciraci, S. Two- and one-dimensional honeycomb structures of silicon and germanium. *Phys. Rev. Lett.* **2009**, *102*, 236804.
- [3] Yang, K. K.; Chen, Y. P.; D'Agosta, R.; Xie, Y. E.; Zhong, J. X.; Rubio, A. Enhanced thermoelectric properties in hybrid graphene/boron nitride nanoribbons. *Phys. Rev. B* **2012**, *86*, 045425.
- [4] Cahangirov, S.; Audiffred, M.; Tang, P. Z.; Iacolino, A.; Duan, W. H.; Merino, G.; Rubio, A. Electronic structure of silicene on Ag(111): Strong hybridization effects. *Phys. Rev. B* **2013**, *88*, 035432.
- [5] Flores, E.; Ares, J. R.; Ferrer, I. J.; Sánchez, C. Synthesis and characterization of a family of layered trichalcogenides for assisted hydrogen photogeneration. *Phys. Status Solidi-Rapid Res. Lett.* **2016**, *10*, 802–806.
- [6] Ferrer, I. J.; Ares, J. R.; Clamagirand, J. M.; Barawi, M.; Sánchez, C. Optical properties of titanium trisulphide ( $\text{TiS}_3$ ) thin films. *Thin Solid Films* **2013**, *535*, 398–401.
- [7] Island, J. O.; Buscema, M.; Barawi, M.; Clamagirand, J. M.; Ares, J. R.; Sánchez, C.; Ferrer, I. J.; Steele, G. A.; van der Zant, H. S. J.; Castellanos-Gomez, A. Ultrahigh photoresponse of few-layer  $\text{TiS}_3$  nanoribbon transistors. *Adv. Opt. Mater.* **2014**, *2*, 641–645.
- [8] Island, J. O.; Barawi, M.; Biele, R.; Almazán, A.; Clamagirand, J. M.; Ares, J. R.; Sánchez, C.; van der Zant, H. S. J.; Álvarez, J. V.; D'Agosta, R. et al.  $\text{TiS}_3$  Transistors with tailored morphology and electrical properties. *Adv. Mater.* **2015**, *27*, 2595–2601.
- [9] Molina-Mendoza, A. J.; Barawi, M.; Biele, R.; Flores, E.; Ares, J. R.; Sánchez, C.; Rubio-Bollinger, G.; Agraït, N.; D'Agosta, R.; Ferrer, I. J. et al. Electronic bandgap and exciton binding energy of layered semiconductor  $\text{TiS}_3$ . *Adv. Electron. Mater.* **2015**, *1*, 1500126.
- [10] Wu, J.; Wang, D.; Liu, H.; Lau, W. M.; Liu, L. M. An *ab initio* study of  $\text{TiS}_3$ : A promising electrode material for rechargeable Li and Na ion batteries. *Rsc Adv.* **2015**, *5*, 21455–21463.
- [11] Barawi, M.; Flores, E.; Ferrer, I. J.; Ares, J. R.; Sánchez, C. Titanium trisulphide ( $\text{TiS}_3$ ) nanoribbons for easy hydrogen photogeneration under visible light. *J. Mater. Chem. A* **2015**, *3*, 7959–7965.
- [12] Jin, Y. D.; Li, X. X.; Yang, J. L. Single layer of  $\text{MX}_3$  ( $M = \text{Ti, Zr}$ ;  $X = \text{S, Se, Te}$ ): A new platform for nano-electronics and optics. *Phys. Chem. Chem. Phys.* **2015**, *17*, 18665–18669.

- [13] Gorlova, I. G.; Zybtev, S. G.; Pokrovskii, V. Y.; Bolotina, N. B.; Verin, I. A.; Titov, A. N. Nonlinear conductivity of quasi-one-dimensional layered compound  $\text{TiS}_3$ . *Phys. B: Condens. Matter* **2012**, *407*, 1707–1710.
- [14] Dai, J.; Zeng, X. C. Titanium trisulfide monolayer: Theoretical prediction of a new direct-gap semiconductor with high and anisotropic carrier mobility. *Angew. Chem., Int. Ed.* **2015**, *54*, 7572–7576.
- [15] Iyikanat, F.; Sahin, H.; Senger, R. T.; Peeters, F. M. Vacancy formation and oxidation characteristics of single layer  $\text{TiS}_3$ . *J. Phys. Chem. C* **2015**, *119*, 10709–10715.
- [16] Aierken, Y.; Çakır, D.; Peeters, F. M. Strain enhancement of acoustic phonon limited mobility in monolayer  $\text{TiS}_3$ . *Phys. Chem. Chem. Phys.* **2016**, *18*, 14434–14441.
- [17] Kang, J.; Wang, L. W. Robust band gap of  $\text{TiS}_3$  nanofilms. *Phys. Chem. Chem. Phys.* **2016**, *18*, 14805–14809.
- [18] Li, M.; Dai, J.; Zeng, X. C. Tuning the electronic properties of transition-metal trichalcogenides via tensile strain. *Nanoscale* **2015**, *7*, 15385–15391.
- [19] Kang, J.; Sahin, H.; Ozaydin, H. D.; Senger, R. T.; Peeters, F. M.  $\text{TiS}_3$  nanoribbons: Width-independent band gap and strain-tunable electronic properties. *Phys. Rev. B* **2015**, *92*, 75413.
- [20] Kang, J.; Sahin, H.; Peeters, F. M. Mechanical properties of monolayer sulphides: A comparative study between  $\text{MoS}_2$ ,  $\text{HfS}_2$  and  $\text{TiS}_3$ . *Phys. Chem. Chem. Phys.* **2015**, *17*, 27742–27749.
- [21] Li, X. R.; Dai, Y.; Li, M. M.; Wei, W.; Huang, B. B. Stable Si-based pentagonal monolayers: High carrier mobilities and applications in photocatalytic water splitting. *J. Mater. Chem. A* **2015**, *3*, 24055–24063.
- [22] Li, X. R.; Dai, Y.; Ma, Y. D.; Liu, Q. Q.; Huang, B. B. Intriguing electronic properties of two-dimensional  $\text{MoS}_2/\text{TM}_2\text{CO}_2$  (TM = Ti, Zr, or Hf) hetero-bilayers: Type-II semiconductors with tunable band gaps. *Nanotechnology* **2015**, *26*, 135703.
- [23] Yun, W. S.; Han, S. W.; Hong, S. C.; Kim, I. G.; Lee, J. D. Thickness and strain effects on electronic structures of transition metal dichalcogenides:  $2\text{H-MX}_2$  semiconductors (M = Mo, W; X = S, Se, Te). *Phys. Rev. B* **2012**, *85*, 033305.
- [24] Conley, H. J.; Wang, B.; Ziegler, J. I.; Haglund, R. F., Jr.; Pantelides, S. T.; Bolotin, K. I. Bandgap engineering of strained monolayer and bilayer  $\text{MoS}_2$ . *Nano Lett.* **2013**, *13*, 3626–3630.
- [25] Wang, C.; Xia, Q. L.; Nie, Y. Z.; Rahman, M.; Guo, G. H. Strain engineering band gap, effective mass and anisotropic dirac-like cone in monolayer arsenene. *AIP Adv.* **2016**, *6*, 035204.
- [26] Island, J. O.; Molina-Mendoza, A. J.; Barawi, M.; Biele, R.; Flores, E.; Clamagirand, J. M.; Ares, J. R.; Sanchez, C.; van der Zant, H. S. J.; D'Agosta, R. et al. Electronics and optoelectronics of quasi-one dimensional layered transition metal trichalcogenides. *2D Materials* **2017**, *4*, 022003.
- [27] Roldán, R.; Castellanos-Gomez, A.; Cappelluti, E.; Guinea, F. Strain engineering in semiconducting two-dimensional crystals. *J. Phys. Condens. Matter* **2015**, *27*, 313201.
- [28] Castellanos-Gomez, A.; Roldán, R.; Cappelluti, E.; Buscema, M.; Guinea, F.; van der Zant, H. S. J.; Steele, G. A. Local strain engineering in atomically thin  $\text{MoS}_2$ . *Nano Lett.* **2013**, *13*, 5361–5366.
- [29] Yang, S. X.; Wang, C.; Sahin, H.; Chen, H.; Li, Y.; Li, S. S.; Suslu, A.; Peeters, F. M.; Liu, Q.; Li, J. B. et al. Tuning the optical, magnetic, and electrical properties of  $\text{ReSe}_2$  by nanoscale strain engineering. *Nano Lett.* **2015**, *15*, 1660–1666.
- [30] Mei, H. X.; Landis, C. M.; Huang, R. Concomitant wrinkling and buckle-delamination of elastic thin films on compliant substrates. *Mech. Mater.* **2011**, *43*, 627–642.
- [31] Vella, D.; Bico, J.; Boudaoud, A.; Roman, B.; Reis, P. M. The macroscopic delamination of thin films from elastic substrates. *Proc. Natl. Acad. Sci. USA* **2009**, *106*, 10901–10906.
- [32] Castellanos-Gomez, A.; Quereda, J.; van der Meulen, H. P.; Agraït, N.; Rubio-Bollinger, G. Spatially resolved optical absorption spectroscopy of single- and few-layer  $\text{MoS}_2$  by hyperspectral imaging. *Nanotechnology* **2016**, *27*, 115705.
- [33] Guan, J.; Song, W. S.; Yang, L.; Tománek, D. Strain-controlled fundamental gap and structure of bulk black phosphorus. *Phys. Rev. B* **2016**, *94*, 045414.
- [34] Giannozzi, P.; Baroni, S.; Bonini, N.; Calandra, M.; Car, R.; Cavazzoni, C.; Ceresoli, D.; Chiarotti, G. L.; Cococcioni, M.; Dabo, I. et al. QUANTUM ESPRESSO: A modular and open-source software project for quantum simulations of materials. *J. Phys. Condens. Matter* **2009**, *21*, 395502.
- [35] Hartwigsen, C.; Goedecker, S.; Hutter, J. Relativistic separable dual-space gaussian pseudopotentials from H to Rn. *Phys. Rev. B* **1998**, *58*, 3641–3662.
- [36] Goedecker, S.; Teter, M.; Hutter, J. Separable dual-space gaussian pseudopotentials. *Phys. Rev. B* **1996**, *54*, 1703–1710.
- [37] Furuseth, S.; Brattas, L.; Kjekshus, A. On the crystal structures of  $\text{TiS}_3$ ,  $\text{ZrS}_3$ ,  $\text{ZrSe}_3$ ,  $\text{ZrTe}_3$ ,  $\text{HfS}_3$ , and  $\text{HfSe}_3$ . *Acta Chem. Scand.* **1975**, *29*, 623–631.